A TOMOGRAPHIC VIEW INTO THE LAYERING OF THE LUNAR REGOLITH. C. Wöhler[1], T. Wilhelm[1], R. Bugiolacchi[2], S. Althoff[1] [1]Image Analysis Group, TU Dortmund University, Otto-Hahn-Str. 4, 44227 Dortmund, Germany (christian.woehler@tu-dortmund.de); [2]Space Science Institute, State Key Laboratory – Planets, Macau University of Science and Technology, Taipa, Macau, China.

Introduction: Recently, the layering of young (<200 Ma) impact ejecta in the region around the landing site of the Chinese lunar spacecraft Chang'E-5 was examined, focusing on the morphometry and the degradation state of small craters with diameters smaller than a few hundred meters [1]. This analysis aimed at identifying the main source craters of the regolith material at the landing site.

In this study, we will extend this framework towards the construction of a three-dimensional, tomographic view of the deposition age of the lunar regolith, where each voxel of the volume is assigned an individual age value. Cross-sections through the volume reveal structures such as buried ejecta blankets that are not accessible by direct analysis of orbital images of the lunar surface.

Data and Method: The first step of our analysis is the automatic detection of small (10-100 m diameter) craters, using the convolutional neural network based small-crater detector of [1-3]. The crater detector relies on a high-resolution digital elevation map (DEM) obtained with the shape from shading based technique of [4] from images acquired by the Lunar Reconnaissance Orbiter Narrow Angle Camera (NAC) [5]. For each detected crater the center position and diameter are estimated, which allows for a straightforward determination of the crater depth from the DEM.

In the second step, the crater size-frequency distribution (CSFD) inferred from the automatic crater detection is modelled with the Monte-Carlo cratering model of [6]. This model considers the diameter-dependent production of impact craters according to [7], counteracted by the destruction of craters by impacts forming overlapping larger craters and by diffusion-induced erosion [8, 9]. The diffusion rate κ is assumed to depend on the crater diameter D and is given by a power law of the form $\kappa(D) = b\, D^a$ [9]. The model estimates the two parameters a and b by adjusting the modeled to the measured CSFD using Bayesian optimization [1].

The third step consists of an estimation of the age of each detected crater based on the depth-to-diameter ratio d/D using the diffusion model. It can be shown that for given d/D, the crater age is proportional to D^{2-a} [3]. For evenly spaced locations in the study area, the distance from all detected craters is computed, and the thicknesses of the ejecta from each crater are derived with the relation of [10]. Based on the known age of each crater, a discretized volume is constructed in which each voxel is assigned a deposition age, resulting in a 3D tomographic view of the regolith layering.

Results: The deposition age of the regolith in the study region (Fig. 1) increases with increasing depth in a strongly variable way (Fig. 2). Vertical cross-sections through the study volume reveal the layering of the regolith and buried structures, such as ejecta deposits of older craters overlaid by younger material (Fig. 3). The cumulative distribution of the inferred crater ages is shown in Fig. 4. The coverage of the method is limited by the age of the oldest crater in the study region.

Conclusion: The developed method appears to be a useful tool for automatic mapping of the regolith layering on atmosphereless planetary bodies.

References: [1] Qian, Y. et al. (2021) GRL 48(20), e95341. [2] Wilhelm, T. and Wöhler, C. (2021) Proc. 2020 IEEE Int. Conf. on Pattern Recognition, pp. 5198-5205. [3] Zhang, F. et al. (2021) JGR Planets 126(8), e06880. [4] Grumpe, A. et al. (2018) in: B. Wu, K. Di, J. Oberst, I. Karachevtseva (eds.), Planetary Remote Sensing and Mapping, CRC Press. [5] Robinson, M. et al. (2010) SSR 150(1-4), 81-124; image data at https://wms.lroc.asu.edu/lroc/search [6] Bugiolacchi, R. and Wöhler, C. (2020) Icarus 350, 113927. [7] Neukum, G. et al. (2001) SSR 96(1/4), 55-86. [8] Fassett, C. I. and Thomson, B. J. (2014) JGR Planets 119(10), 2255-2271. [9] Fassett, C. I. et al. (2018) LPSC XLIX, abstract 1502. [10] Huang, J. et al. (2018) JGR Planets 123(7), 1684-1700.

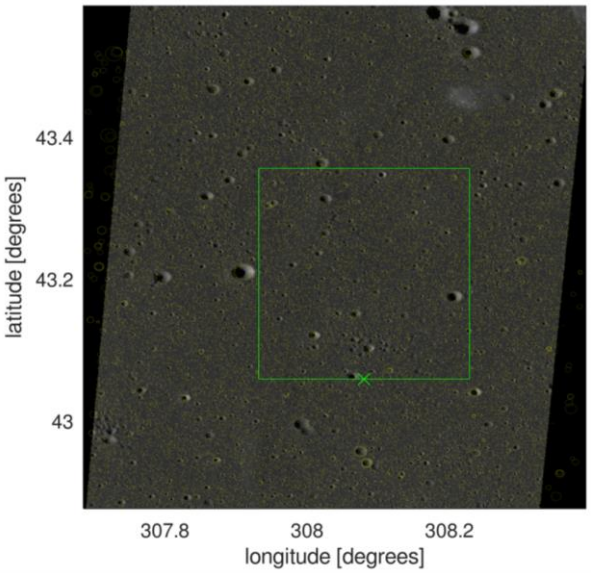

Fig. 1: Part of NAC image M1173414625 of the area around the Chang'E-5 landing site (cross, see [1]). Detected craters are marked by yellow circles. The green box corresponds to the region analyzed in Figs. 2 and 3.

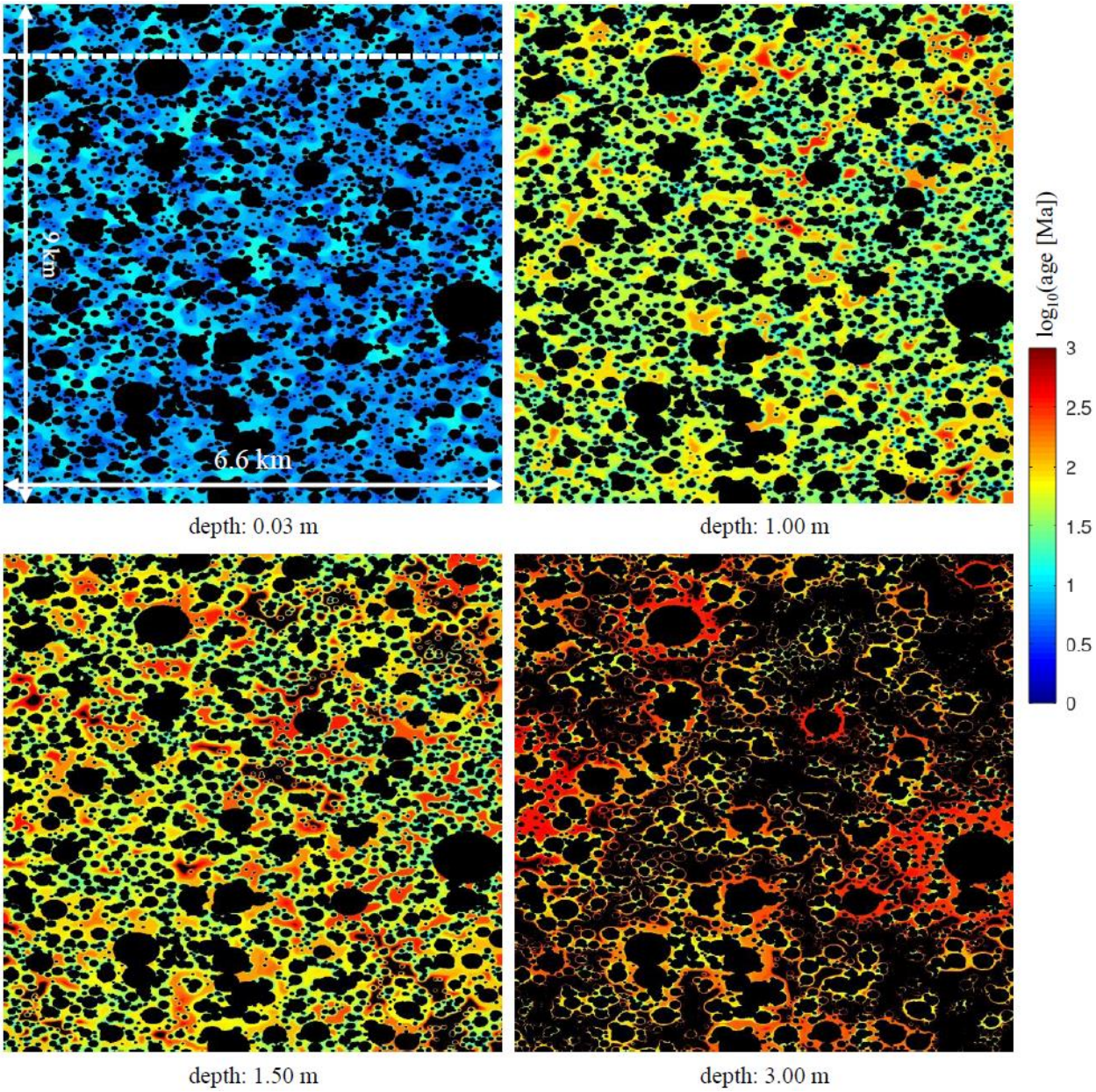

Fig. 2: Deposition age of the regolith in the study region (box in Fig. 1) at different depths below the surface. A circular area with a diameter of two crater diameters around each crater center was omitted from the analysis. Black denotes unavailable data.

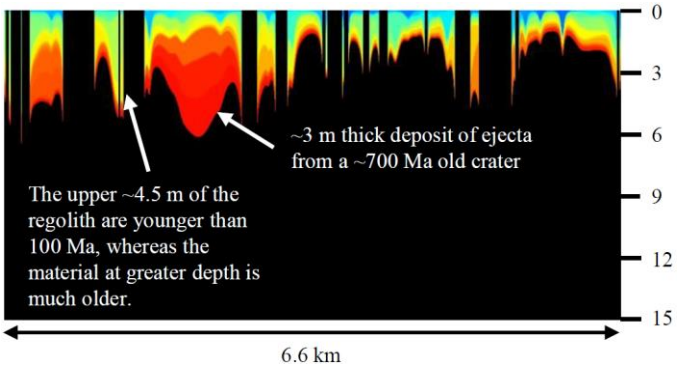

Fig. 3: Vertical cross-section along the dashed line marked in Fig. 1. Black denotes unavailable data.

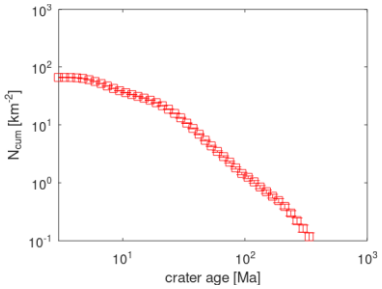

Fig. 4: Cumulative distribution of the ages inferred for the detected craters based on the diffusion model.